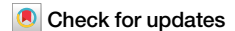
A Nature Portfolio journal



https://doi.org/10.1038/s42003-025-08642-3

Multi-omics insights of immune cells in the risk and prognosis of idiopathic membranous nephropathy



Xiaoyi Song^{1,2,3,7}, Wen Zhu^{1,2,7}, Yang Li^{4,7}, Zhanyu Li⁵, Wanwei Cao⁵, Jieyu Lu^{1,2}, Wanping Pan^{1,2}, Jingyue Wei^{1,2} & Man Li **⊕** ^{1,2,6} ⋈

Idiopathic membranous nephropathy (IMN) is the major cause of autoimmune-related nephrotic syndrome. The role immune cells play in the risk and prognosis of IMN remains elusive. We employ multi-omics data and a variety of approaches to evaluate the causal link between 731 immune-cell phenotypes and IMN. In light of the findings emanating from Mendelian randomization analyses, only the regulatory T cell (Treg) subtype (CD39⁺ Tregs) survived from Bonferroni correction and is causally related to IMN. These cells are significantly enriched in the IMN microenvironment and are negatively correlated with treatment response and prognosis. We validate our findings through multiple immunofluorescence staining and explore the characteristics of CD39⁺ Tregs using Single-cell transcriptome analysis and flow cytometry. Based on the signature genes of CD39⁺ Tregs, we construct 107 composited machine-learning models to identify MN. We show the substantial contribution of CD39⁺ Tregs in both the risk factor determination and prognosis of IMN.

Membranous Nephropathy (MN), the leading cause of nephrotic syndrome (NS) in non-diabetic adults¹ has a global incidence of 12 cases per million annually².³. Concurrently, idiopathic membranous nephropathy (IMN) is an affliction experienced by up to 80% of MN patients⁴.⁵ characterized by immune deposit formation alongside complement-mediated proteinuria. Despite significant advancements in the understanding of IMN pathogenesis over the past decade³, its prevalence continues to rise, making it the second most common primary glomerulonephritis⁶ and a major contributor to end-stage renal disease patients⁵.

IMN reflects a pathological condition characterized by the dysregulation of the immune system⁸. Immune cells operate as the catalysts for auto-inflammatory responses in IMN, in addition to creating immune deposits and the complement. Consequently, immunotherapy has long been recognized as an essential treatment methodology for IMN⁹. For instance, Rituximab, a monoclonal anti-CD20 antibody, has significantly enhanced the complete remission (CR) rate of IMN by eliminating excessive B cells¹⁰. However, the roles of immune cells in the pathogenesis of IMN remain partially elusive, and their the immunomodulatory activity require further elucidation. Investigating the underpinning

mechanisms between immune cells and IMN will advance diagnostics, treatment strategies, and prognostic evaluations for IMN.

With the advancement of multi-omics technology and an increasing repository of pertinent data, a unique opportunity presents itself to dissect multi-factorial phenotypes, regulatory processes, and response patterns of immune cells in IMN. Previous observational studies have attempted to characterize the immune microenvironment in IMN, yielding several intriguing results^{11,12}. However, there is minimal evidence elucidating the causal relationship between immune-cell phenotypes and IMN. Moreover, discerning the clinical relevance of this relationship might lead to more individualized treatment strategies for IMN.

In this study, we integrated multi-omics data to scrutinize the correlation between immune-cell phenotypes and IMN. Utilizing batched two-sample bidirectional Mendelian Randomization (MR), we first examined the causal link between 731 immune-cell phenotypes and IMN. Proceeding from causality, we sequentially immune regulatory landscape and evaluated how immune-cell phenotypes influence the disease status and clinical outcome. Our comprehensive approach systematically elucidates diagnostic and prognostic

¹Guangdong Provincial Engineering Research Center of Molecular Imaging, the Fifth Affiliated Hospital, Sun Yat-sen University, Zhuhai, 519000, China. ²Guangdong-Hong Kong-Macao University Joint Laboratory of Interventional Medicine, the Fifth Affiliated Hospital, Sun Yat-sen University, Zhuhai, 519000, China. ³Department of Nasopharyngeal Cancer Control and Prevention Center, the Fifth Affiliated Hospital, Sun Yat-sen University, Zhuhai, 519000, China. ⁴Department of Cardiothoracic Surgery, the Fifth Affiliated Hospital, Sun Yat-sen University, Zhuhai, 519000, China. ⁵Department of Pathology, the Fifth Affiliated Hospital, Sun Yat-sen University, Zhuhai, 519000, China. ⁵These authors contributed equally: Xiaoyi Song, Wen Zhu, Yang Li. ⊠e-mail: liman26@mail.sysu.edu.cn

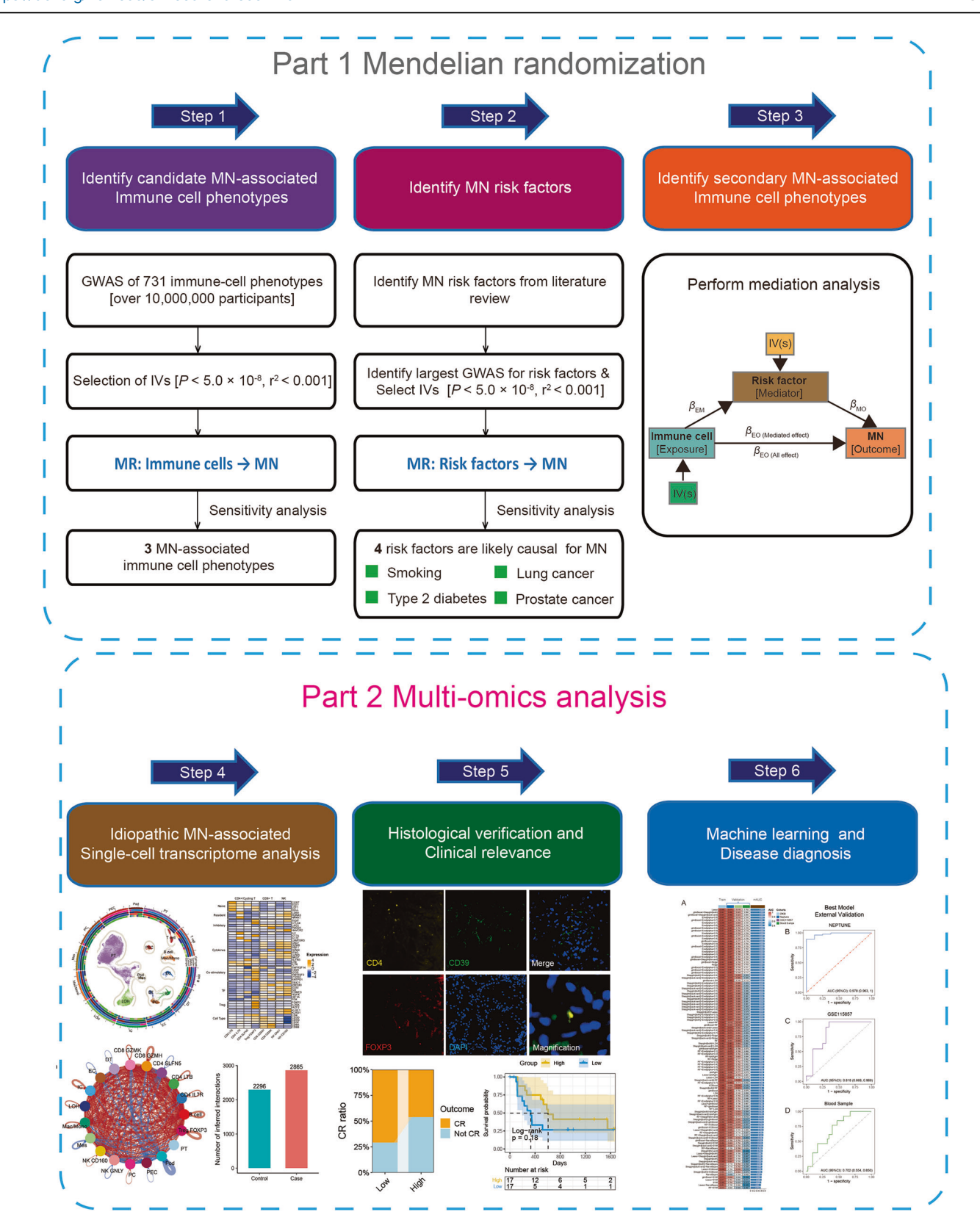


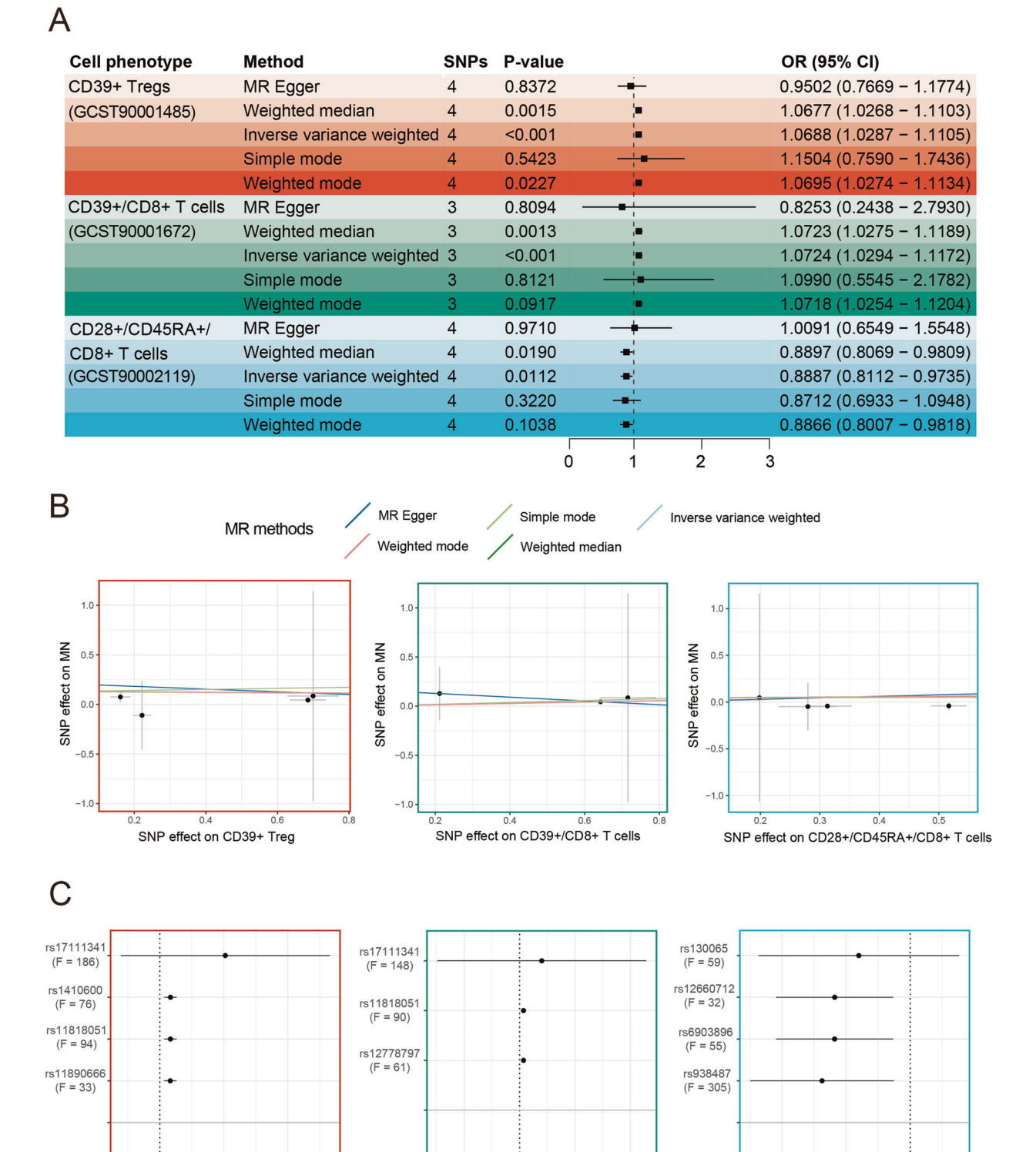
Fig. 1 | Study design and workflow of this study. MN membranous nephropathy, GWAS genome-wide association study, IV instrumental variable, CR complete remission.

immune cell - IMN relationships, shedding light on potential biomarker and therapeutic targets.

Materials and methods

The comprehensive workflow of the present study is delineated in Fig. 1. This study received approval from the Institutional Review Board of the

Fifth Affiliated Hospital of Sun Yat-sen University (Ethical approval number: 2024-S-11), and written informed consent was obtained from all the patients recruited in this study. All ethical regulations relevant to human research participants were followed. All supplementary tables of this study are available in the Supplementary Data 1 file. For MR analysis, a STROBE-MR checklist¹³ was presented in Supplementary Table 1.



MR leave-one-out sensitivity analysis for

'CD39+/CD8+ T cells' on 'MN'

Fig. 2 | Mendelian randomization analyses evaluate the causal association between positive immune-cell phenotypes and MN. A Forest plots to visualize the causal effects of positive immune-cell phenotypes with MN in terms of different MR methods. B Scatter plots to visualize the effect of harmonized SNPs with positive

MR leave-one-out sensitivity analysis for

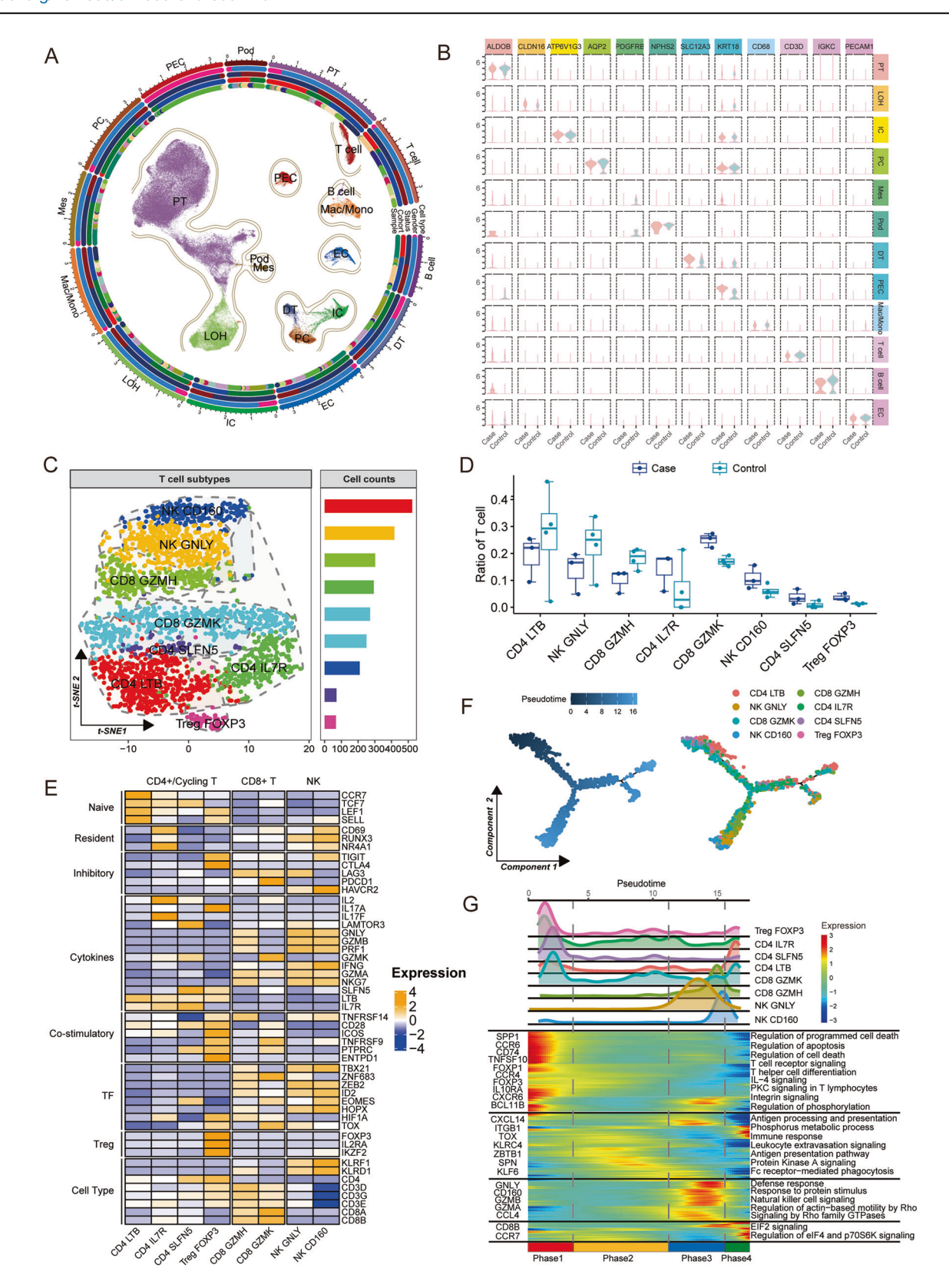
'CD39+ Treg' on 'MN'

immune-cell phenotypes and MN. C MR leave-one-out sensitivity analyses for positive immune-cell phenotypes on MN. SNP Single-nucleotide polymorphism, OR odds ratio, CI confidence interval, MN membranous nephropathy, MR Mendelian randomization, F F-statistic value.

MR leave-one-out sensitivity analysis for

' CD28+/CD45RA+/CD8+ T cells' on 'MN'

All



GWAS data source

A published GWAS summary dataset was obtained from IEU OpenGWAS project as the main outcome dataset that consisted of 2150 European MN cases and 5829 European healthy controls¹⁴. The immune-cell-phenotype datasets were also obtained from IEU OpenGWAS project and regarded as

the main exposure, with a total of 3757 European subjects included¹⁵. It included the most diverse immune-cell phenotypes and a considerable sample size throughout the available data. A summary of the GWAS datasets and resources pertinent to this study is given in Supplementary Tables 2-3.

Fig. 3 | Single-cell transcriptome analysis delineates the landscape of T-cell population in the immune microenvironment of IMN. A UMAP plot showing the distribution of cell types in the IMN ecosystem from the integrated scRNA-seq datasets included in this study. B Violin plots showing the selected marker genes that were used to identify the cell types in this study. The relative expression level of these genes was compared between IMN samples and healthy kidneys. Case, IMN; Control, healthy kidney. C t-SNE projections of sub-clustered T cells, labeled in different colors. D Boxplots illustrating the fraction of T-cell subtypes in IMN (n = 9) and healthy kidney (n = 6), respectively. The two groups were labeled in different colors. Case, IMN; Control, healthy kidney. The P-value was calculated by the Wilcoxon test. The error bars represent the error margins. E Heatmap indicating the

expression of selected gene sets in T-cell subtypes, including naive, resident, inhibitory, cytokines, co-stimulatory, transcriptional factors (TF), and cell types. F Pseudotime-ordered analysis of T-cell subtypes from IMN and healthy samples. T cell subtypes are labeled by colors. G Heatmap showing the dynamic changes in gene expression of T-cell subtypes along the pseudotime (lower panel). The distribution of T-cell subtypes during the transition (divided into 4 phases), along with the pseudo-time. Subtypes are labeled by colors (upper panel). IMN idiopathic membranous nephropathy, PT proximal tubule cells, LOH loop of Henle cells, IC intercalated cells, PC principal cells, Mes mesangial cells, Pod podocytes, DT distal tubule cells, PEC parietal epithelial cells, Mac macrophages, Mono monocytes, EC endothelial cells, Treg regulatory T cell.

Nephrotic transcriptome cohorts

From the European Renal cDNA Bank (ERCB) cohort^{16,17}, we obtained whole-genome glomerular microarray expression profiles for 223 subjects (21 MN patients) and tubulointerstitial expression profiles for 219 subjects (18 MN patients). For the Nephrotic Syndrome Study Network (NEPTUNE) cohort^{18,19}, we scrutinized microarray profiles from two sets: the initial cohort 125 subjects (48 MN patients) and an additional 160 subjects (43 MN patients), yielding 71 MN subjects after deduplication. We validated our findings using a published RNA-seq cohort²⁰ (GSE115857) with 86 subjects (11 MN patients). Additionally, we acquired expression profiles via RNA sequencing conducted on blood samples from 53 subjects (13 MN patients) collected from the Fifth Affiliated Hospital of Sun Yat-sen University.

Systematic MR screening for the causal immune-cell phenotype of MN and MN risk factors

The associations between immune-cell phenotypes and target outcomes (MN or MN risk factors) were estimated using Two-sample MR²¹. The genetic variants used as IV should exceed our prespecified thresholds $(P < 5 \times 10^{-8})$ with biomarker, variants pruned if $r^2 > 0.001$). To avoid weak instrumental variable bias, we evaluated the SNP-exposure association strengths using the F statistic (F>10), and a minor allele frequency (MAF) > 0.01 was applied to eliminate rare variants and prevent confounding results (Supplementary Table 4). All statistical power for each instrumental variable was estimated using "mRnd"22. Additionally, instrumental variables from the human leukocyte antigen (HLA) region were excluded due to their strong pleiotropic effects. To assess the robustness of our results, several sensitivity analyses were employed: (i) Cochran Q test for heterogeneity²³; (ii) MR-Egger's intercept for horizontal pleiotropy²⁴; (iii) influential outlier IVs due to pleiotropy were identified using MR Pleiotropy Residual Sum and Outlier (MR-PRESSO)²⁵. We used multiple MR methods (MR Egger, Weighted median, Simple mode, and Weighted mode) to calculate the MR estimates.

We employed a two-sample MR framework incorporating the sensitivity analyses for both primary MR (immune-cell phenotypes \rightarrow MN) and two-step MR (Step-1 MR: MN risk factors \rightarrow MN; Step-2 MR: immune-cell phenotypes \rightarrow MN risk factors). Effects on binary or quantitative outcomes are reported as odds ratios (ORs) with their 95% confidence intervals (CIs). All statistical tests were two-sided and considered statistically significant at $P_{\text{CausalEstimate}} \leq 6.84 \times 10^{-5}$ (Bonferroni-corrected P value for 731 immune-cell phenotypes: 0.05/731 = 6.84 \times 10 $^{-5}$), $P_{\text{Q-stat}} \geq$ 0.05, $P_{\text{Egger-Intercept}} \geq$ 0.05, and $P_{\text{GlobalTest}} \geq$ 0.05. For the final positive immune phenotypes and risk factors, a bidirectional MR analysis was conducted to verify the directional causality with MN. All statistical analyses were performed using "Two-SampleMR" R package 21 .

Mediation analysis

If there is a causal correlation between an immune-cell phenotype and both MN as well as risk factors, a mediation analysis was executed. For each established risk factor of secondary MN that we examined (Hepatitis B/C²⁶, Hashimoto thyroiditis⁴, Lung cancer²⁷, Prostate cancer²⁷, Rheumatoid arthritis²⁸, Systemic lupus erythematosus²⁸, Type 2 diabetes²⁸, Nonsteroidal

anti-inflammatory drugs²⁹, Obesity³⁰, and Hypertension³⁰), instrumental variables were derived from GWAS summary statistics restricted to European populations (Supplementary Table 2-3). We utilized the Product method to ascertain the beta value of the indirect effect and the Delta method to compute the standard error and the CI³¹.

Single-cell transcriptome analysis

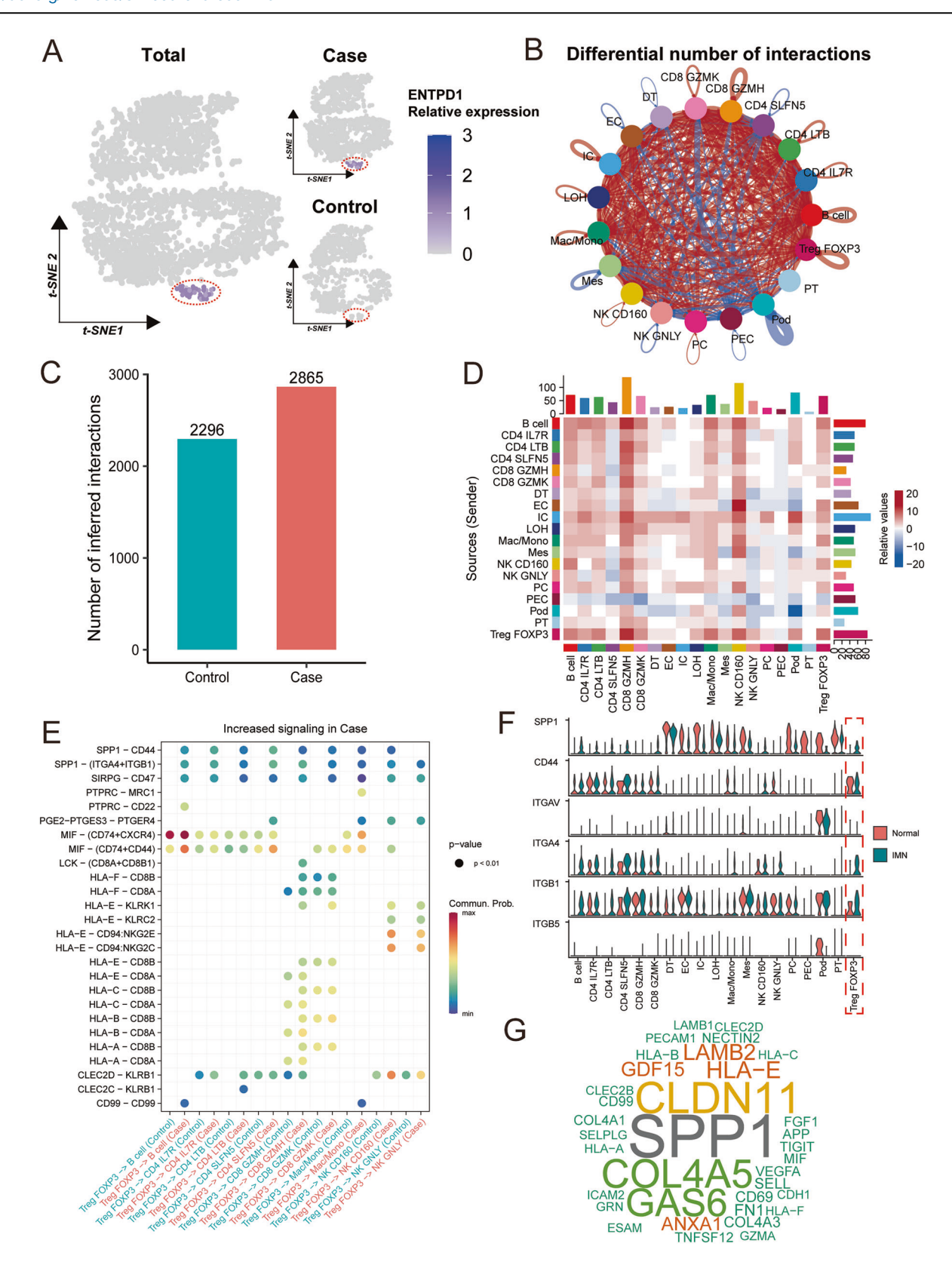
A total of three publicly available scRNA-seq datasets (GSE17145811, GSE241302¹², and GSE131685³²) were obtained, including 9 patients with IMN and 6 healthy donors. For each dataset, a uniform analysis pipeline -MAESTRO³³ was adopted to perform quality control, batch effect removal, data integration, clustering, and cell-type annotation. The criteria of cellular quality assessment were as follows¹: 200 <nFeatures <7000²; mitochondrial gene ratio < 30%. Cells were categorized according to their respective marker genes previously reported in the literature 11,12. The doublets were filtered by the R package "DoubletFinder"³⁴. The biological trajectories of cells were analyzed by the R package "Monocle"35. The cell-cell paracrine communications analysis was performed using "CellChat"36. Significant interactions were selected with a *P*-value < 0.05. Genes related to the immune-cell phenotype were identified using the "FindMarkers" function with default parameters. The significant differential expression genes (adjusted Pvalue < 0.05 and average fold-change > 1) were collected to perform the gene set enrichment analysis (GSEA). The immune-cell phenotype signature score was calculated using the "GSVA" package³⁷. The top 20 phenotyperelated genes were derived from the differential gene analysis of the scRNAseq analysis. We utilized the Gene Set Variation Analysis (GSVA) method to compute the signature score. The "gsva" function was utilized, setting parameters as¹: method = "ssgsea"²; kcdf = "Gaussian"³; min.sz = 10. This was done to calculate the normalized enrichment scores in individual samples for a representation of the enrichment of a specific immune population.

Diagnostic marker-based prediction model development and validation

A total of 12 extensively used machine learning algorithms, namely Lasso, Ridge, Enet, Stepglm, SVM, glmBoost, LDA, plsRglm, RandomForest, GBM, XGBoost, and NaiveBayes, were employed to develop an efficient tissue-to-blood classification prediction model utilizing selected biomarkers. A total of 107 combination methodologies were implemented in the final calculation of the models. To train the models, ERCB was selected as the reference dataset. For external validation, we utilized expression profiles from tissue samples in NEPTUNE and GSE115857, as well as blood samples of patients with MN or healthy donors collected locally. Evaluations of the models' performance were undertaken by calculating the area underneath each model's Receiver Operating Characteristic curve (AUROC) and subsequently representing the results visually through heatmaps.

Multiple immunofluorescence staining

A total of 6 biopsy tissues of IMN and 6 normal donors were obtained from the Fifth Affiliated Hospital of Sun Yat-sen University along with 13 IMN biopsies of 7 IMN patients who achieved CR (24-hour proteinuria <0.3 g



with stable renal function at 6 months) and 6 IMN patients who did not achieve CR before Rituximab treatment. Paraffin-embedded tissue sections were completely dewaxed in xylene and subsequently rehydrated using a series of ethanol gradients. Antigen retrieval was performed by heating the sections for 15 minutes at 95 - 98°C in sodium citrate buffer. The sections were then incubated overnight at 4°C with primary antibodies. Once

complete, the slide was further incubated with a primary antibody cocktail containing anti-CD4 (1:100, ab183685, Abcam, UK), anti-CD39 (1:100, 11-0399-42, Invitrogen, USA), and anti-FOXP3 (1:100, 14-5773-82, Invitrogen, USA), at 4°C overnight. Subsequently, the tissues were incubated using secondary antibody cocktails containing Alexa Fluor 647 (1:500, 4414S, CST, USA), Alexa Fluor 555 (1:500, 4417S, CST), and Alexa Fluor 488

Fig. 4 | **Differential analysis of cell communication of immune environment between IMN and healthy kidney.** A *t*-SNE plot showing the relative expression level of ENTPD1 (the coding gene for CD39) in Tregs within the microenvironment of IMN and healthy kidneys. Case, IMN; Control, healthy kidney. **B** Circle plot showing the differential number of cell-cell interactions among various cell types in the microenvironment between IMN and healthy kidney. The color red indicates the increased interactions, while the color blue represents the decreased interactions. **C** Barplot compares the total number of inferred cell-cell interactions within the microenvironment of IMN and healthy kidney. Case, IMN; Control, healthy kidney. **D** Heatmap visualizes the differential number of ligand-receptor interactions among different cell populations between IMN and healthy kidneys. The rows represent the signaling senders' interactions, and the columns represent the signaling receivers'

interactions. E Bubble plot showing the differential dysfunctional signaling of regulatory T cells with other immune populations in microenvironment of IMN and healthy kidney by comparing the communication probabilities. Case, IMN; Control, healthy kidney. F Violin plots showing the expression level of *SPP1*-related signaling genes among various cell types in the microenvironment between IMN and healthy kidney. G Wordcloud plot visualizes the differentially enriched signal in IMN compared to the healthy kidney. IMN idiopathic membranous nephropathy, PT proximal tubule cells, LOH loop of Henle cells, IC intercalated cells, PC principal cells, Mes mesangial cells, Pod podocytes, DT distal tubule cells, PEC parietal epithelial cells, Mac macrophages, Mono monocytes, EC endothelial cells, Treg regulatory T cell.

(1:500, 4408S, CST, USA) for 60 min at room temperature. Finally, the Panorama pathological scanner (3DHISTECH Ltd., Hungary) was used to capture tissue images, while HALO software (version 3.5) was used for processing image data. The cell ratio is defined as the count of a specific celltype occupies the count of all the cells observed in a slide.

Flow cytometry sorting and IL-10 enzyme-linked immunosorbent assay

We collected around 5 ml blood samples from 5 patients with IMN and 5 healthy donors to extract the peripheral blood mononuclear cells, respectively. Red blood cells were removed by LymphoprepTM (07851, STEM-CELL, Germany). Afterwards, the cells were diluted to 5×10⁷/mL in PBS containing 2%FBS and 1 mM EDTA. Next, we used EasySepTM Human CD4+CD127lowCD25+ Regulatory T Cell Isolation Kit (18063, STEM-CELL, Canada) and EasySepTM Magnet (18000, STEMCELL, Canada) to sort the regulatory T cells (Tregs) from PBMC. Cells were stained with the anti-CD39 (1:200, 11-0399-42, Invitrogen, USA), which is an antibody with pre-labeled. Then, these Tregs were sorted on BD FACSaria (BD Biosciences, USA), and the CD39⁺ cells (Tregs) were obtained for further cell culture. Flow cytometric analysis was performed and analyzed using CytExpert V2.5 software (Beckman Coulter, USA). For the identification of cell populations and visualization in this paper, cells were stained with the corresponding antibodies after fixation/permeabilization. We used a primary antibody cocktail containing anti-CD4 (1:200, ab183685, Abcam, UK) and anti-FOXP3 (1:200, 14-5773-82, Invitrogen, USA) following by a secondary antibody cocktail containing Alexa Fluor 647 (1:500, 4414S, CST, USA), Alexa Fluor 555 (1:500, 4417S, CST, USA) to stain the Tregs. The gating strategy was as followed: Inital gating on a forward scatter area (FSC-A) versus forward scatter height (FSC-H) plot was performed to exclude cell doublets and aggregates, ensuring analysis was restricted to single cells. CD39⁺ Tregs were defined with thresholds established using appropriate isotype controls (>104). Gating boundaries were determined using unstained controls, fluorescence-minus-one controls, and isotype controls to ensure specificity and minimize background noise. We mainly used the histograms to draw the gating boundaries for visualization and the dot plot was used to sorting the target cell population.

For IL-10 enzyme-linked immunosorbent assay, we collected the CD39⁺ Tregs and used the ImmunoCult[∞]-XF Medium (10981, STEM-CELL, Canada) to culture them. After a 5-day cultivation, we examined the concentration of IL-10 in the cell culture medium by Human IL-10 ELISA Kit (EH0009, HUABIO, China). The optical density was examined using a Varioskan LUX Multimode Microplate Reader (Thermo, USA) set to 450 nm corrected with 570 nm.

RNA sequencing

We collected blood samples from 23 patients with nephrotic syndrome and 30 healthy donors to perform RNA sequencing. All participants were recruited from the Fifth Affiliated Hospital of Sun Yat-sen University and have provided informed consent which was approved by the Institutional Review Board of the Fifth Affiliated Hospital, Sun Yat-sen University. Total RNA extraction, transcriptome sequencing, and data analysis were

conducted as previously reported³⁸. The process was detailed in Supplementary Methods.

Statistics and reproducibility

Statistical analysis was performed using R software (version 4.2.1). Continuous data were compared using Student's t-test or Kruskal–Wallis test. Categorical data were analyzed using Chi-square test or Fisher's exact test. The diagnostic efficiency of models was mainly quantified by the AUC. The CI of AUC was calculated using 10,000 bootstrap replicates. Kaplan-Meier curves between survival groups were compared by log-rank test. For all statistical tests, a P < 0.05 was considered statistically significant. The flow cytometry sorting and IL-10 enzyme-linked immunosorbent assay experiments were conducted for three replicates to ensure to guarantee reproducibility.

Reporting summary

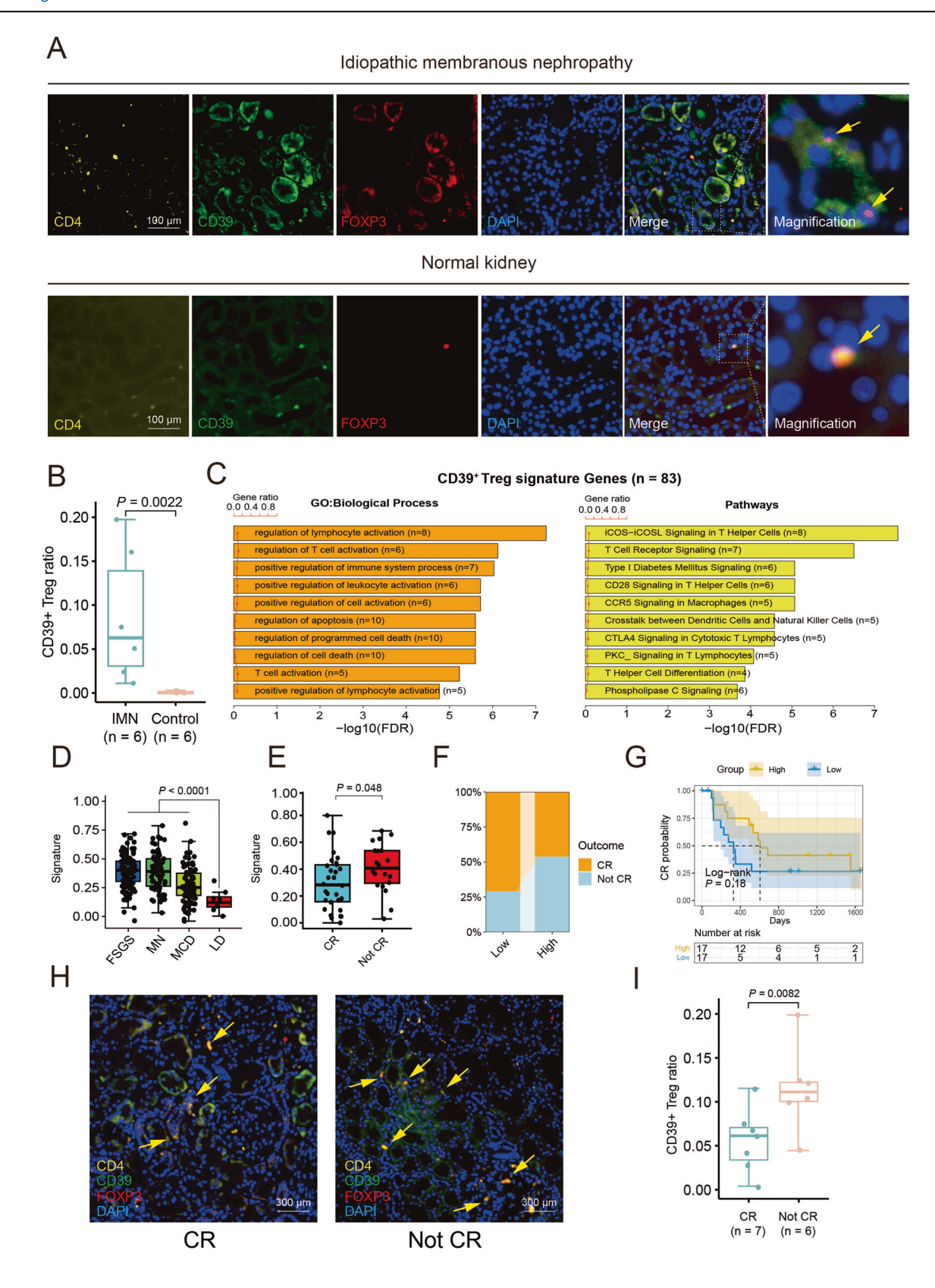
Further information on research design is available in the Nature Portfolio Reporting Summary linked to this article.

Results

Identification of IMN-associated immune-cell phenotypes

A comprehensive analysis of 731 immune-cell phenotypes was conducted to ascertain their causal relationships with MN. Initially, three immune-cell phenotypes were deemed as potentially causal (Fig. 2A): CD39 $^+$ Tregs, CD39 $^+$ & CD8 $^+$ T cells, and CD28 $^+$ & CD45RA $^+$ & CD8 $^+$ T cells. Sensitivity analyses further substantiate the causal associations (Fig. 2B, C) through only CD39 $^+$ Treg survived Bonferroni correction ($P=6.54\times10^{-5}$). The STROBE-MR checklist and all procedure files (Supplementary Table 4-8) of MR analyses can be found in Supplemental Material, and there were no IVs that showed horizontal pleiotropy and heterogeneity. Genetic predisposition to CD39 $^+$ Treg enrichment is correlated with an increased risk of MN (OR [95%CI] = 1.068 [1.0284, 1.110]). The reverse MR analysis showed no significant effects of MN on these immune cell phenotypes (Supplementary Tables 9–13).

To decipher the prospective causal mechanisms that link the putative causal immune-cell phenotype with MN, we implemented a two-step MR analysis focusing on conventional MN risk factors. Initially, we executed MR analyses to delineate the causal interactions of the risk factors with MN. Subsequently, we evaluated the causal repercussions of the putative causal immune-cell phenotype on the underscored risk factors. Among all potential mediators, type 2 diabetes had the strongest positive impact on MN (OR [95% CI] = 1.78 [1.45, 2.19], Supplementary Fig. 1) in "Step-1" MR analysis. Both lung and prostate cancer demonstrated a positive correlation with MN (OR [95% CI] = 1.51 [1.48, 1.54] and OR [95% CI] = 1.54 [1.44, 1.64], Supplementary Fig. 1). Interestingly, smoking showed a negative correlation with MN (OR [95%] = 2×10^{-4} [1×10^{-4} , 6×10^{-4}]). The remaining risk factors had no significant effects on MN (P > 0.05). Additionally, no evidence supported the reverse causal association from MN to any candidate risk factors (Supplementary Table 13). Nevertheless, the "Step-2 MR" analysis detected no correlation between the MN-associated immune-cell phenotype (CD39⁺ Treg) and any of the three emphasized MN risk factors



(Supplementary Table 13), suggesting ${\rm CD39^+}$ Treg could be an immune-cell phenotype primarily associated with IMN.

Tregs in the immune microenvironment of IMN

We next examined the T cells in an integrated single-cell transcriptome dataset (9 IMN and 6 controls, 121,824 cells). After quality control, around

27% of the cells were filtered mainly due to the high expression of mitochondrial genes. A total of 89,129 cells were included in the final downstream analysis. Before clustering, batch correction was conducted based on "Sample ID" (Supplementary Fig. 2). The landscape of single-cell profiles is depicted in Fig. 3A. Cell populations were categorized based on established marker genes (Fig. 3B). We isolated all T cells (2408 cells) for subpopulation

Fig. 5 | Characteristics of CD39⁺ Treg and the clinical relevance with MN.

A Immunofluorescence images showing the distribution of CD39⁺ Tregs in IMN and healthy kidney, using antibodies CD4, FOXP3, and CD39. Scale bars, 100 µm. **B** Boxplots showing the fraction of CD39⁺ Tregs in IMN (blue) and healthy kidney (red) samples calculated by the regions of interest from immunofluorescence images. The CD39⁺ Treg ratio was defined as the count of CD39⁺ Tregs occupies the count of all the cells observed in a slide. The *P*-value was calculated by the Wilcoxon test. The error bars represent the error margins. **C** Bar chart showing the enrichment of specific biological processes and signaling pathways of CD39⁺ Tregs, based on the signature gene set consisting of the marker genes of CD39⁺ Tregs obtained from the single-cell transcriptome data. The scale bars and line charts were integrated to show the proportion of genes (accounting for the 83 genes) that were enriched in each GO term or pathway. **D** Boxplots showing the CD39⁺ Tregs signature scores of different pathological groups of nephrotic syndrome and normal kidney samples in the NEPTUNE dataset. The error bars represent the error margins. **E** Boxplot showing the CD39⁺ Tregs signature scores of the complete remission (CR) group and that of

the not-CR group. The error bars represent the error margins. F Stacked bar plot showing the CR ratio in high-score and low-score groups (grouped by the median of CD39⁺ Tregs signature score). G Kaplan-Meier analysis shows the CR rate of patients with the time spent on treatment, characterized by either low (blue) or high (yellow) CD39+ Tregs signature scores. H Immunofluorescence images showing the distribution of CD39⁺ Tregs in tissue slides of patients who achieved CR or did not after Rituximab treatment, using antibodies CD4, FOXP3, and CD39. Scale bars, 300 μm. I Boxplots showing the fraction of CD39⁺ Tregs in CR (blue) and Not-CR (red) IMN samples calculated by the regions of interest from immunofluorescence images. The CD39⁺ Treg ratio was defined as the count of CD39⁺ Tregs occupies the count of all the cells observed in a slide. The P-value was calculated by the Wilcoxon test. The error bars represent the error margins. The median CR time, the number of patients, and the risk classification are indicated in the figure. Significance was calculated using the log-rank test. MN membranous nephropathy, IMN idiopathic membranous nephropathy, FSGS focal segmental glomerular sclerosis, MCD minimal change disease, LD live donor, CR complete remission.

analysis. The re-clustering of T cells unveiled 8 distinct populations (Fig. 3C). All subtypes were shared across patients and between IMN and normal specimens. A comparison of T-cell subtypes ratios showed no significant differences between the IMN and normal group. Notebly, Tregs frequency in IMN samples was not higher than in normal kidneys (Fig. 3D). The characteristics of these T-cell subpopulations are shown in Fig. 3E.

Next, we investigated immune state dynamics and cellular transitions in T cells infiltrating in MN. (Fig. 3F). Intriguingly, Tregs surfaced earlier than the other T-cell subtypes along the trajectory (Fig. 3G), suggesting their potential role in regulating the immune microenvironment during the initial onset of IMN. By identifying the transitional genes and conducting pathway analysis, we characterized the transcriptional changes in intermediate T-cell states. T cells trajectories in IMN comprised four distinct phases (Fig. 3G). Functional genes of Tregs, such as *FOXP3*, *IL10RA*, and *SPP1*, were highly expressed in T cells at the initial state.

The role of Tregs in cell-cell interactions of IMN

The CD39⁺ Tregs were identified by the expression of *ENTPD1* (the coding gene of CD39). If the expression of ENTPD1 was not zero in a Treg, we then classified this Treg as a CD39+ Treg. The scRNA-seq data indicated a predominant enrichment of CD39⁺ Tregs in the IMN samples, contrasting with their near absence in the normal kidneys (Fig. 4A). We subsequently examined differential cellular interactions and ligand-receptor pathways in the microenvironment of IMN and normal samples. Relative to the normative state, there was a significant escalation in cell-to-cell interactions within the disease state (Fig. 4B) with 569 new interactions identified in IMN compared to the normal samples (Fig. 4C). As shown in Supplementary Fig. 3, most of the increased pathways in IMN are immunologically related. Additionally, the PARs-related pathways³⁹ exhibited up-regulation in IMN, with IMN's hypercoagulability and thrombosis risk. Conversely, the interaction of podocytes was diminished in IMN, while the interaction between podocytes and immune cells was enhanced (Fig. 4D), consistent with the prevalent podocyte damage in IMN⁴⁰.

Further cell-type-specific analysis revealed Tregs exhibited high activities as both sender and receiver of ligand-receptor conductors. Compared to the normal kidney, *SPP1* was identified as the primarily upregulated secretory protein mediated by Tregs in IMN microenvironment (Fig. 4E). Tregs in IMN primarily utilized the *SPP1-CD44* and *SPP1-(ITGA4+ITGB1)* (Fig. 4E and Supplementary Fig. 4). Consistently, *SPP1*-related signaling maintained its ranking at the top when compared to all other increasing ligand-receptor pathways in IMN (Fig. 4F), indicating that Tregs could significantly impact the process of renal fibrosis of IMN.

CD39⁺ Tregs signature development and the clinical relevance

To validate our earlier findings of CD39⁺ Tregs enrichment in IMN, we performed multiple immunofluorescence staining on kidney biopsies from 6 IMN patients and 6 healthy donors (Fig. 5A). Analysis of comparative data

unveiled a significant enrichment of CD39 $^+$ Tregs within the IMN microenvironment (Fig. 5B). For a more in-depth understanding of CD39 $^+$ Tregs, we identified a total of 83 signature genes through differential gene analysis (Supplementary Table 14) which were prominently associated with immunomodulation-related biological processes and Treg-related signaling (Fig. 5C). Utilizing the GSVA algorithm, we constructed a signature score using the top 20 signature genes (ranked by fold change) to quantify CD39 $^+$ Tregs enrichment. We calculated the signature scores via the microarray expression profiles from the NEPTUNE dataset across diverse phenotypes (Supplementary Table 15). The signature score in each pathological type of NS was significantly elevated compared to normal kidney tissue (P < 0.0001, Fig. 5D).

As for clinical parameters, patients who eventually achieved CR exhibited lower signature scores compared to those who could not achieve CR post-treatment (P=0.048, Fig. 5E). Using the median signature scores (median threshold = 0.363) as a cutoff, we stratified patients into high- and low-score groups. The CR rate was substantially higher in the low-score group (74% vs 49%, P=0.12, Fig. 5F), and time to CR was shorter (median 325 vs 617 days, P=0.18, Fig. 5G). The low-score group possessed a relatively higher eGFR level (P=0.16, Supplementary Fig. 5A) and slightly lower proteinuria (P=0.39, Supplementary Fig. 5B) compared to the high-score group. For external validation, we procured kidney biopsy samples from 13 additional IMN patients (7 CR vs 6 non-CR) by multiple immunofluorescence staining (Fig. 5H). CR patients maintained lower CD39⁺ Treg ratio (P=0.0082, Fig. 5I). These findings were subsequently corroborated in our in-house RNA-seq cohort (Supplementary Fig. 6).

The immunosuppressive function of CD39⁺ Tregs and its correlation with renal fibrosis

To further investigate the immunosuppressive function of CD39⁺ Tregs, we isolated CD39+ Tregs from the blood of patients with IMN and healthy donors (Fig. 6A and Supplementary Figs. 7 and 8). We compared the ability of IL-10 secretion of CD39⁺ Tregs in blood of 5 IMN patients with 5 healthy donors. The results showed that the CD39⁺ Tregs in IMN patients secreted more IL-10 than those in donors (P = 0.011, Fig. 6B), suggesting a more powerful immunosuppressive function of CD39⁺ Tregs in IMN patients. Meanwhile, in order to examine the potential association between CD39⁺ Tregs and renal fibrosis, we calculated the kidney fibrotic microenvironment (FME) score⁴¹ to evaluate the degree of fibrosis in IMN patients within ERCB and NEPTUNE cohorts. The Spearman correlation analysis showed the signature scores were significantly relevant to the FME scores (Fig. 6C, D). Then, we further divided the patients into high-score and low-score groups by the median of the FME scores of patients in NEPTUNE cohort (median threshold = 3.077). Approximately 60% of patients in the low-score group achieved CR, compared to only 35% in the high-score group (P = 0.11, Fig. 6E). In addition, the high-score group spent more time than low-score group to reach CR (P = 0.01, Fig. 6F).

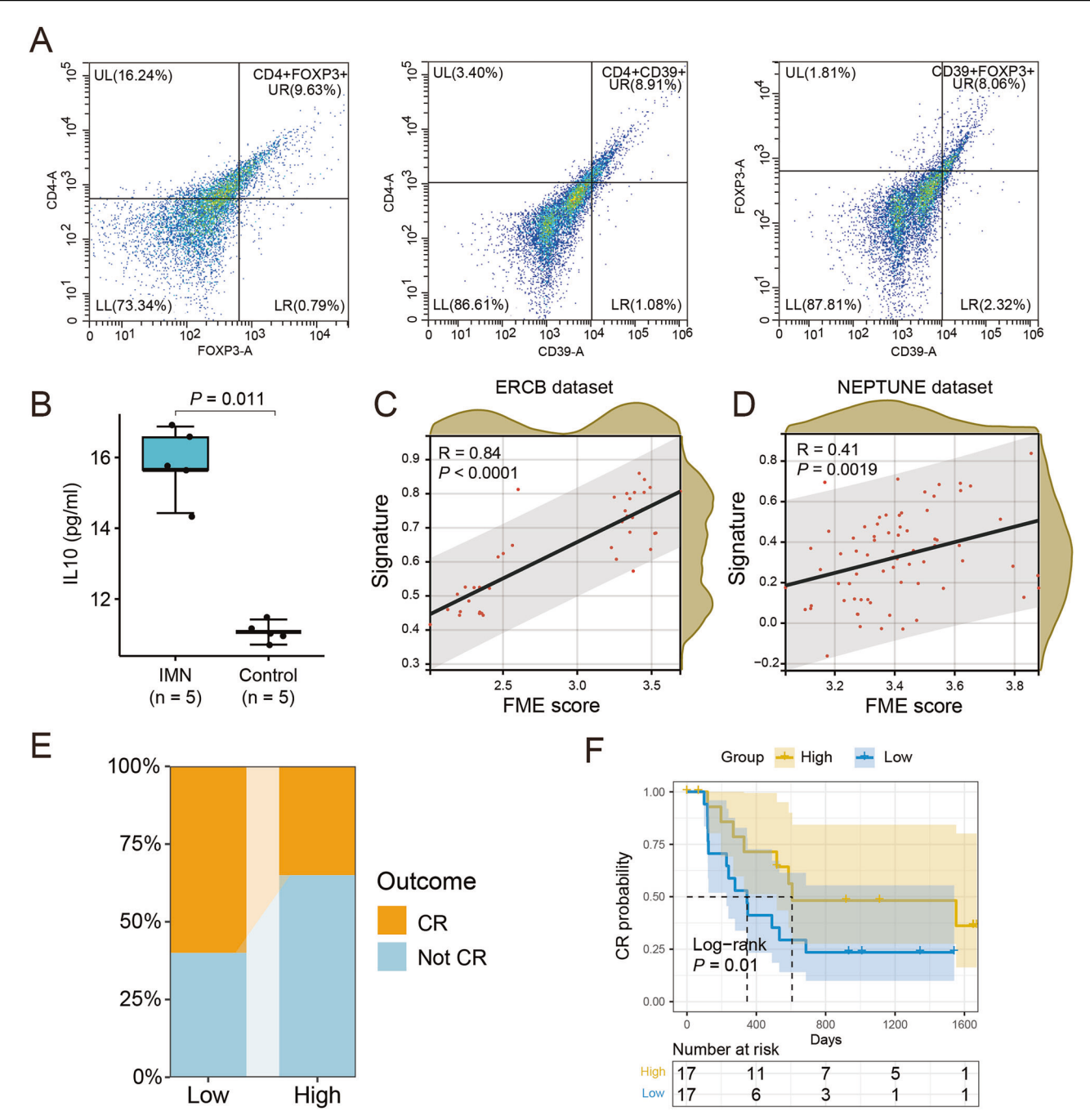


Fig. 6 | CD39⁺ Tregs have a stronger immunosuppressive function in IMN patients and is associated with the fibrosis process. A Flow cytometry sorting of CD39⁺ Treg cells. B Boxplots showing the IL-10 secretion concentration (pg/ml) of CD39⁺ Tregs in IMN (blue) patients and healthy donors (red). The error bars represent the error margins. C Scatter plot showing the Spearman correlation between the CD39⁺ Tregs signature score and the FME score in patients with MN of ERCB dataset. D Scatter plot showing the Spearman correlation between the CD39⁺

Tregs signature score and the FME score in patients with IMN of NEPTUNE dataset. E Stacked bar plot showing the CR ratio in high-score and low-score groups (grouped by the median of FME score). F Kaplan—Meier analysis shows the CR rate of patients with the time spent on treatment, characterized by either low (blue) or high (yellow) FME scores. FME fibrotic microenvironment, MN membranous nephropathy, CR complete remission.

CD39⁺ Tregs signature genes can be used as a potential diagnostic marker to identify MN

To expand the usage of CD39⁺ Tregs signature genes to help distinguish MN from normal kidney and other pathological types of NS, we aimed to develop a diagnostic model. By using the ERCB cohort as the training set, we evaluated 107 machine-learning models across various external validation cohorts, calculating average AUC values for each. The clinical characteristics of the development and external validation cohorts were presented in Supplementary Tables 16–19. The Lasso algorithm demonstrated the most

effective model performance with a mean AUC of 0.833 across validation cohorts. The best model was constructed by 21 selected signature genes (Supplementary Table 20), including 11 candidates without previously established mechanistic link to IMN (Supplementary Table 21). The pathway enrichment analysis of the selected genes was showed in Supplementary Fig. 9. The most effective model achieved high AUCs for different cohorts: 0.978 (95% CI: 0.963–1.00) for NEPTUNE cohort (a kidney-tissue microarray and mRNA-seq cohort, Fig. 7B), 0.818 (95% CI: 0.668–0.969) for GSE115857 (a kidney-tissue mRNA-seq cohort, Fig. 7C), and 0.702 (95%

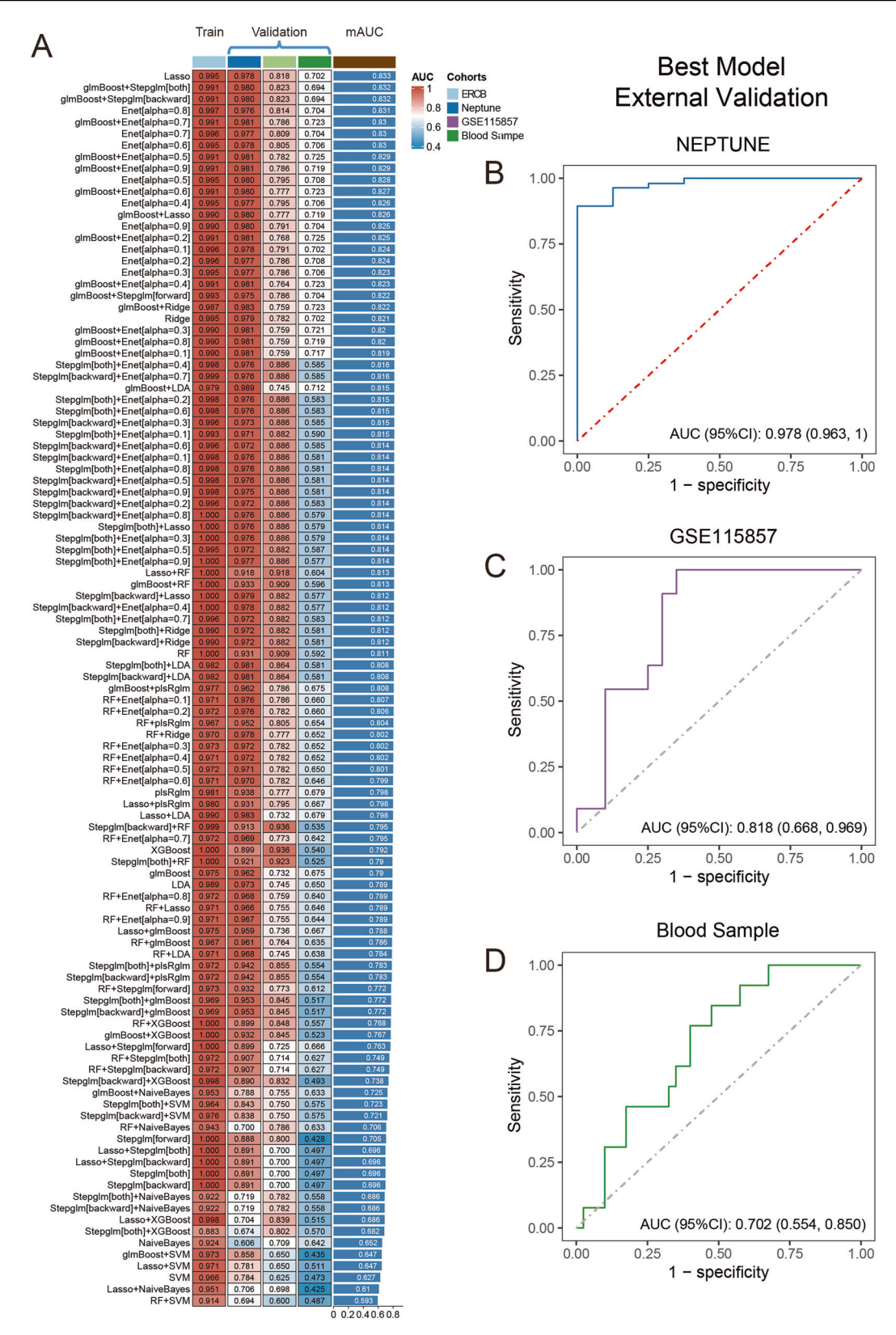


Fig. 7 | Construction and validation of the MN diagnostic model based on CD39⁺ Tregs signature genes. A The area under ROC curve (AUC) values of 107 machine-learning algorithm combinations in the development cohort and three external validation cohorts. B The ROC curve of the best model in the NEPTUNE dataset.

C The ROC curve of the best model in the GSE115857 dataset. **D** The ROC curve of the best model in the Blood Sample dataset was generated in this study. The AUC value and the corresponding 95% confidence interval are labeled.

CI: 0.554–0.850) for our blood sample cohort (a blood mRNA-seq cohort, Fig. 7D). Moreover, the CD39⁺ Tregs signature genes could also be used to diagnose NS with machine learning methods in blood samples using 35 signature genes (Supplementary Table 20) with the best AUC around 0.7 (Supplementary Fig. 10A-D).

Discussion

In this study, we systematically explored the causal relationship between 731 immune-cell phenotypes and MN. The significant role of CD39⁺ Tregs in both the risk factor determination and pathogenesis of IMN was revealed and elucidated by the integrative multi-omics analysis. CD39⁺ Tregs significantly correlate with clinical outcomes in IMN patients, establishing CD39⁺ Tregs as a prognostic biomarker for disease progression and treatment response. Moreover, the CD39⁺ Tregs gene signature showed good diagnostic accuracy for MN and NS in blood-based testing.

Kidney injury can be an inadvertent consequence of systemic immune disorders. Immune cells sustain peripheral tolerance to circulating antigens, including the immune complexes⁴². The critical intersection positions immune cell as key contributor to the advancement of kidney diseases, spanning acute kidney injury to chronic kidney disease. A comprehensive investigation into the relationship between immune cells and IMN could provide novel insights into disease mechanisms and therapeutic targets for IMN.

The pathogenesis of IMN involves both circulating immune network complexes and auto-reactive immune cells activation directed toward healthy kidney cells⁴³. Despite antibodies being secreted by B cells, the significant contribution of T cells to the immune system cannot be overlooked. As upstream of B cells, the imbalance of T cells prompts the immunological pathological state of IMN. A thorough understanding of T cell subsets is therefore necessary for a comprehensive explanation of B cell subset modifications. Our study found that CD39⁺ Treg is indispensable not only to the pathogenesis of IMN but also to its appropriate clinical treatment.

Tregs play a significant role in immunosuppression by responding uniquely to diverse immune reactions and environments⁴⁴. Our research focused on a specific Treg subtype (CD39⁺ Tregs) that is more prevalent in IMN than in healthy kidneys. Previous studies have revealed that CD39⁺ Tregs have a more powerful immunosuppressive function than CD39⁻ Tregs among autoimmune diseases^{45,46}. In this study, our research focused on a specific Treg subtype (CD39⁺ Tregs) that is more prevalent in IMN than in healthy kidneys. Meanwhile, we revealed that the CD39+ Tregs in blood of IMN patients secreted more IL-10 than those in donors. These CD39⁺ Tregs regulate the immune network of IMN primarily through the SPP1 - CD44 and SPP1 - (ITGA4 + ITGB1) pathways. The increased co-expression and interaction between SPP1⁺ immune cells and Tregs had been revealed in the CD44-enriched region⁴⁷. SPP1 is correlated to the development of pathological fibrosis, which is a key pathological alteration in the progression of MN⁴⁸. Previous studies have revealed that Tregs were associated with tissue fibrosis in chronic tissue injury⁴⁹. They overexpressed markers of hyperactivation and fibrosis in the fibrotic environment and were suspected to aggravate renal fibrosis^{50,51}. In this study, we found the immunosuppressive function of CD39⁺ Tregs in IMN patients was more powerful than those in healthy individuals. However, they were significantly correlated with renal fibrosis and associated with a worse prognosis. In addition, they were also suspected to be related to the treatment resistance of Rituximab. The increase of CD39⁺ Tregs could be a pathological and physiological change that occurs during the compensatory to decompensated stage of this disease.

Our clinical analyses revealed that lower CD39⁺ Tregs ratio were associated with poorer treatment response and worse clinical outcomes in MN patients. While current diagnostic standards depend on invasive renal biopsy⁵², we developed a machine learning-based diagnostic model using CD39⁺ Tregs signature genes. The model demonstrated excellent diagnostic capabilities in external validation and offers the potential for non-invasive blood-based MN detection. All these findings revealed a potential usage of CD39⁺ Tregs in the diagnosis and treatment.

Our study has several limitations. Firstly, we could not perform stratified analyses due to the lack of individual-level data, potentially overlooking variations between different groups. Secondly, we observed variable performance of our diagnostic models across independent validation cohorts. This inter-cohort variability may be caused by technical heterogeneity in sequencing platforms and biological differences between sample types (kidney tissue vs. blood). Moreover, there was still the absence of a suitable method to estimate the sample power of different analyses in this study. Finally, a comprehensive interpretation of the CD39⁺ Tregs and their function in IMN's microenvironment necessitates additional experimental exploration.

The clinical implementation of our diagnostic models for MN and NS will require validation through extensive blood-based cohort studies to enhance their reliability, coupled with optimization of the gene signature to develop a streamlined PCR-based blood assay requiring fewer than 10 target genes for improved diagnostic accessibility. Additionally, targeting depletion of CD39⁺ Tregs could potentially overcome Rituximab resistance and reduce treatment duration in IMN, while immunomodulatory approaches targeting these cells might attenuate renal fibrosis progression. However, excessive CD39⁺ Treg reduction could disrupt immune homeostasis, necessitating further research to establish optimal therapeutic windows and precise modulation strategies for maintaining their beneficial immunosuppressive functions while mitigating profibrotic effects.

In conclusion, applying a multi-omics causality approach has enabled us to highlight the causal link between CD39⁺ Treg and IMN. The knowledge gathered from our findings serves as a significant resource for enriching the understanding of immune-cell-related risk and prognostic effect in IMN.

Data availability

The summary-level data of GWAS used in this study are publicly available (https://gwas.mrcieu.ac.uk/ and http://ftp.ebi.ac.uk/pub/databases/gwas/ summary statistics/). Detailed information on these data can be found in Supplementary Table 1 and the STROBE-MR checklist (Supplementary Data 1). Single-cell transcriptomic data were downloaded from Gene Expression Omnibus (GSE171458, GSE241302, and GSE131685). NEP-TUNE and ERCB data are available at Nephroseq.org and through the Gene Expression Omnibus (GSE104954, GSE104948, GSE182380, GSE104066, GSE133288, GSE197307). The previously published MN-related RNA-seq cohort can be obtained from GSE115857. The RNA-seq data of blood samples generated in this study have been deposited in the GSA human database (https://ngdc.cncb.ac.cn) under accession number HRA008427. The numerical source data behind the Figures of this study can be found in Supplementary Data 2 file. All data that support the findings of this study are available online and can be obtained from the corresponding author upon reasonable request.

Received: 23 December 2024; Accepted: 31 July 2025; Published online: 10 August 2025

References

- Ronco, P. et al. Membranous nephropathy. Nat. Rev. Dis. Prim. 7, 69 (2021).
- Couser, W. G. Primary membranous nephropathy. Clin. J. Am. Soc. Nephrol. 12, 983–997 (2017).
- Mcgrogan, A., Franssen, C. F. & De Vries, C. S. The incidence of primary glomerulonephritis worldwide: a systematic review of the literature. Nephrol. Dial. Transpl. 26, 414–430 (2011).
- Cattran, D. C. & Brenchley, P. E. Membranous nephropathy: integrating basic science into improved clinical management. *Kidney Int* 91, 566–574 (2017).
- Ronco, P. & Debiec, H. Pathophysiological advances in membranous nephropathy: time for a shift in patient's care. *Lancet* 385, 1983–1992 (2015).

- Maisonneuve, P. et al. Distribution of primary renal diseases leading to end-stage renal failure in the United States, Europe, and Australia/ New Zealand: results from an international comparative study. Am. J. Kidney Dis. 35, 157–165 (2000).
- Avasare, R., Andeen, N. & Beck, L. Novel antigens and clinical updates in membranous nephropathy. *Annu. Rev. Med.* 75, 219–332 (2024).
- Nieto-Gañán, I. et al. Revisiting immunological and clinical aspects of membranous nephropathy. *Clin. Immunol.* 237, 108976 (2022).
- Kidney Disease Improving Global Outcomes (KDIGO) Glomerular
 Diseases Work Group. KDIGO 2021 Clinical Practice Guideline for the
 Management of Glomerular Diseases. Kidney Int 100, S1–S276 (2021).
- Gauckler, P. et al. Rituximab in membranous nephropathy. Kidney Int. Rep. 6, 881–893 (2021).
- Xu, J. et al. Single-Cell Profiling Reveals Transcriptional Signatures and Cell-Cell Crosstalk in Anti-PLA2R Positive Idiopathic Membranous Nephropathy Patients. Front. Immunol. 12, 683330 (2021).
- Shi, M. et al. Single-cell RNA sequencing shows the immune cell landscape in the kidneys of patients with idiopathic membranous nephropathy. Front Immunol. 14, 1203062 (2023).
- Skrivankova, V. W. et al. Strengthening the reporting of observational studies in epidemiology using mendelian randomization: The STROBE-MR Statement. JAMA 326, 1614–1621 (2021).
- Xie, J. et al. The genetic architecture of membranous nephropathy and its potential to improve non-invasive diagnosis. *Nat. Commun.* 11, 1600 (2020).
- Orrù, V. et al. Complex genetic signatures in immune cells underlie autoimmunity and inform therapy. *Nat. Genet* 52, 1036–1045 (2020).
- Yasuda, Y. et al. European Renal cDNA Bank (ERCB) Consortium.
 Gene expression profiling analysis in nephrology: towards molecular definition of renal disease. Clin. Exp. Nephrol. 10, 91–98 (2006).
- Schmid, H. et al. Modular activation of nuclear factor-kappaB transcriptional programs in human diabetic nephropathy. *Diabetes* 55, 2993–3003 (2006).
- Gadegbeku, C. A. et al. Design of the Nephrotic Syndrome Study Network (NEPTUNE) to evaluate primary glomerular nephropathy by a multidisciplinary approach. *Kidney Int.* 83, 749–756 (2013).
- Barisoni, L. et al. Digital pathology evaluation in the multicenter Nephrotic Syndrome Study Network (NEPTUNE). Clin. J. Am. Soc. Nephrol. 8, 1449–1459 (2013).
- Shao, F. et al. Causal association of plasma circulating metabolites with nephritis: a Mendelian randomization study. Front Nutr. 11, 1364841 (2024).
- 21. Hemani, G. et al. The MR-Base platform supports systematic causal inference across the human phenome. *Elife* **7**, e34408 (2018).
- Brion, M. J., Shakhbazov, K. & Visscher, P. M. Calculating statistical power in Mendelian randomization studies. *Int. J. Epidemiol.* 42, 1497–1501 (2013).
- Yavorska, O. O. & Burgess, S. MendelianRandomization: an R package for performing Mendelian randomization analyses using summarized data. *Int. J. Epidemiol.* 46, 1734–1739 (2017).
- Bowden, J., Davey, S. G. & Burgess, S. Mendelian randomization with invalid instruments: effect estimation and bias detection through Egger regression. *Int. J. Epidemiol.* 44, 512–525 (2015).
- Verbanck, M. et al. Detection of widespread horizontal pleiotropy in causal relationships inferred from Mendelian randomization between complex traits and diseases. *Nat. Genet* 50, 693–698 (2018).
- Couser, W. G. & Johnson, R. J. The etiology of glomerulonephritis: roles of infection and autoimmunity. *Kidney Int.* 86, 905–914 (2014).
- Leeaphorn, N. et al. Prevalence of cancer in membranous nephropathy: a systematic review and meta-analysis of observational studies. Am. J. Nephrol. 40, 29–35 (2014).

- Floege, J. et al. Management and treatment of glomerular diseases (part 1): conclusions from a Kidney Disease: Improving Global Outcomes (KDIGO) Controversies Conference. Kidney Int 95, 268–280 (2019).
- Hogan, J. J., Markowitz, G. S. & Radhakrishnan, J. Drug-induced glomerular disease: immune-mediated injury. *Clin. J. Am. Soc. Nephrol.* 10, 1300–1310 (2015).
- Ponticelli, C. & Glassock, R. J. Glomerular diseases: membranous nephropathy–a modern view. *Clin. J. Am. Soc. Nephrol.* 9, 609–616 (2014).
- Carter, A. R. et al. Mendelian randomisation for mediation analysis: current methods and challenges for implementation. *Eur. J. Epidemiol.* 36, 465–478 (2021).
- 32. Liao, J. et al. Single-cell RNA sequencing of human kidney. *Sci. Data* **7**. 4 (2020).
- 33. Wang, C. et al. Integrative analyses of single-cell transcriptome and regulome using MAESTRO. *Genome Biol.* **21**, 198 (2020).
- Bernstein, N. J. et al. Solo: doublet identification in single-cell RNA-Seq via semi-supervised deep learning. *Cell Syst.* 11, 95–101.e5 (2020).
- Cao, J. et al. The single-cell transcriptional landscape of mammalian organogenesis. *Nature* 566, 496–502 (2019).
- 36. Jin, S. et al. Inference and analysis of cell-cell communication using CellChat. *Nat. Commun.* **12**, 1088 (2021).
- Hänzelmann, S., Castelo, R. & Guinney, J. GSVA: gene set variation analysis for microarray and RNA-seq data. *BMC Bioinform.* 14, 7 (2013).
- 38. Chung, M. et al. Best practices on the differential expression analysis of multi-species RNA-seq. *Genome Biol.* **22**, 121 (2021).
- Zelaya, H. et al. Nucleic acid sensing promotes inflammatory monocyte migration through biased coagulation factor VIIa signaling. *Blood* 143, 845–857 (2024).
- Jiang, H. et al. Understanding the podocyte immune responses in proteinuric kidney diseases: from pathogenesis to therapy. Front. Immunol. 14. 1335936 (2024).
- Abedini, A. et al. Single-cell multi-omic and spatial profiling of human kidneys implicates the fibrotic microenvironment in kidney disease progression. *Nat. Genet* 56, 1712–1724 (2024).
- 42. Kant, S. et al. Advances in understanding of pathogenesis and treatment of immune-mediated kidney disease: a review. *Am. J. Kidney Dis.* **79**, 582–600 (2022).
- 43. Motavalli, R. et al. Immune system-mediated cellular and molecular mechanisms in idiopathic membranous nephropathy pathogenesis and possible therapeutic targets. *Life Sci.* **238**, 116923 (2019).
- 44. Zhao, Q. et al. Helper T cells in idiopathic membranous nephropathy. *Front Immunol.* **12**, 665629 (2021).
- Ortiz, M. A. et al. Altered CD39 and CD73 expression in rheumatoid arthritis: implications for disease activity and treatment response. *Biomolecules* 14, 1 (2023).
- do Sacramento, P. M. et al. Major depression favors the expansion of Th17-like cells and decrease the proportion of CD39+Treg cell subsets in response to myelin antigen in multiple sclerosis patients. Cell Mol. Life Sci. 79, 298 (2022).
- 47. Zhang, Q. et al. Integration of single-cell RNA sequencing and bulk RNA transcriptome sequencing reveals a heterogeneous immune landscape and pivotal cell subpopulations associated with colorectal cancer prognosis. Front. Immunol. 14, 1184167 (2023).
- Li, L. et al. Proteomic landscape of the extracellular matrix in the fibrotic kidney. Kidney Int 103, 1063–1076 (2023).
- Loffredo, L. F., Savage, T. M., Ringham, O. R. & Arpaia, N. Treg-tissue cell interactions in repair and regeneration. *J. Exp. Med.* 221, e2023124405032024c (2024).
- Kurawaki, S. et al. Mesenchymal stem cells pretreated with interferongamma attenuate renal fibrosis by enhancing regulatory T cell induction. Sci. Rep. 14, 10251 (2024).

- Jang, J. Y. et al. Interleukin-2/anti-interleukin-2 immune complex attenuates cold ischemia-reperfusion injury after kidney transplantation by increasing renal regulatory T cells. *Clin. Transl. Med.* 14, e1631 (2024).
- Kidney Disease Improving global outcomes (KDIGO) CKD Work Group. KDIGO 2024 clinical practice guideline for the evaluation and management of chronic kidney disease. *Kidney Int.* 105, S117–S314 (2024).

Acknowledgements

The authors are grateful to Yang Li research group of Guangdong Provincial Engineering Research Center of Molecular Imaging for providing partially necessary reagents and equipment to support this study. This study is funded by grants from the National Natural Science Foundation of China (Grant No. 82000628) and the Guangdong-Hong Kong-Macao University Joint Laboratory of Interventional Medicine Foundation of Guangdong Province (Grant No. 2023LSYS001). The authors have full control, and funders played no role in the design, analysis, or interpretation of this work.

Author contributions

Guarantors of integrity of the entire study, X.Y.S., W.Z., Y.L., Z.Y.L., W.W.C., J.Y.L., W.P.P., J.Y.W., M.L.; study concepts/study design or data acquisition or data analysis/interpretation, X.Y.S., W.Z., Y.L., M.L.; manuscript drafting or manuscript revision for important intellectual content, X.Y.S., M.L.; approval of final version of submitted manuscript, all authors; agrees to ensure any questions related to the work are appropriately resolved, all authors; literature research, X.Y.S., W.Z., Y.L., M.L.; clinical studies, X.Y.S., W.Z., Y.L., W.W.C., J.Y.L., W.P.P., J.Y.W., M.L.; experimental studies, X.Y.S., W.Z., Y.L., M.L.; statistical analysis, X.Y.S., M.L.; and manuscript editing, X.Y.S., W.Z., Y.L., M.L. X.Y.S., W.Z., Y.L., and M.L. have verified the underlying data used in this study.

Competing interests

The authors declare no competing interests.

Additional information

Supplementary information The online version contains supplementary material available at https://doi.org/10.1038/s42003-025-08642-3.

Correspondence and requests for materials should be addressed to Man Li.

Peer review information *Communications Biology* thanks the anonymous reviewers for their contribution to the peer review of this work. Primary Handling Editors: Jian-Da Lin and Joao Valente.

Reprints and permissions information is available at http://www.nature.com/reprints

Publisher's note Springer Nature remains neutral with regard to jurisdictional claims in published maps and institutional affiliations.

Open Access This article is licensed under a Creative Commons Attribution-NonCommercial-NoDerivatives 4.0 International License, which permits any non-commercial use, sharing, distribution and reproduction in any medium or format, as long as you give appropriate credit to the original author(s) and the source, provide a link to the Creative Commons licence, and indicate if you modified the licensed material. You do not have permission under this licence to share adapted material derived from this article or parts of it. The images or other third party material in this article are included in the article's Creative Commons licence, unless indicated otherwise in a credit line to the material. If material is not included in the article's Creative Commons licence and your intended use is not permitted by statutory regulation or exceeds the permitted use, you will need to obtain permission directly from the copyright holder. To view a copy of this licence, visit https://creativecommons.org/licenses/by-nc-nd/4.0/.

© The Author(s) 2025